FINAL REPORT

The Use of Anisotropic Dielectric Materials for Obtaining Mutual Capacitance

Duke University
Department of Electrical Engineering
Durham, North Carolina

Period Covered by Project
June 1964 - June 1966

ARO-D Project No. 5115-E
Grant No. DA-ARO-D-31-124-G581

Theo C. Pilkington
Robert B. Roe

June 1, 1966

Requests for additional copies by Agencies of the Department of Defense, their contractors, and other Government agencies should be directed to:

Defense Documentation Center
Cameron Station
Alexandria, Virginia 22314

Department of Denfense contractors must be established for DDC services or have their "need-to-know" certified by the cognizant military agency of their project or contract.

All other persons and organizations should apply to the:

U. S. Department of Commerce
Office of Technical Services
Washington 25, D. C.

LIST OF PUBLICATIONS AND PARTICIPATING PERSONNEL

Publications

1. Pilkington, T. C. and Roe, R. B., "Analysis of Fields in Anisotropic Media with Application to the Anisotropy Transformer," Proc. IEEE, Vol. 53, No. 6, June 1965, p653-54.

Participating Personnel

Dr. Theo C. Pilkington

Mr. Robert B. Roe – M. S. thesis (A Study of Fields in Anisotropic Dielectric Materials) supported by this project.

ERRATA

p. 4	Equation 5 equals zero
p. 10	Principal axes carry single prime
p. 16	From Figure 5, it is seen
p. 19	Figure 6 – Temp. is in °C.
p. 35	Figure 14 – ORDINATE – "TRANSFER RATIO"
p. 38	Figure 16 – ORDINATE – "OUTPUT VOLTAGE"
p. 61	Second Reference pp. 643-44

CONTENTS

LIST OF FIGURES

The Use of Anisotropic Dielectric Materials for Obtaining Mutual Capacitance

Chapter I

INTRODUCTION

The use of anisotropic dielectric materials to achieve mutual capacitance was first proposed by C. P. Gadsden (1963,a,b). A physical realization termed the anisotropy transformer was described and an open-circuit voltage gain was predicted but not realized experimentally (Loh, 1963).

In the investigation reported here, a generalized theoretical analysis of the anisotropy transformer and similar devices is developed. A transform-analog technique for the determination of optimum physical configurations for realization of mutual capacitance and voltage gain and for the determination of equivalent-circuit parameters is employed. The open-circuit voltage gain of the anisotropy transformer is shown to have an upper limit of unity under linear operation conditions and this demonstration is extended to include the general class of such devices.

Since a linear-mode gain greater than unity is impossible, the non-linear properties of multi-terminal dielectric materials (specifically Rochelle salt) and their application as nonlinear elements in dielectric amplifier configurations is investigated. The use of Rochelle salt as a nonlinear element proves to be impractical and feasibility of nonlinear anisotropic coupling techniques in other oriented ferroelectric crystals is found to

depend on poorly understood aspects of the macroscopic consequences of the mechanism of polarization reversal.

Chapter II

LINEAR ANISOTROPIC COUPLING

Coordinate Transformations

In an anisotropic dielectric the relation between the displacement vector and the electric field intensity is

$$\bar{D} = \varepsilon_0 \bar{E} + \bar{P} = \bar{\bar{\varepsilon}}\, \bar{E} \tag{1}$$

where $\bar{P}$ is the polarization and $\bar{\bar{\varepsilon}}$ a second rank permittivity tensor. Equation (1) is not valid in materials exhibiting a spontaneous polarization. In Cartesian coordinates, for the case in which only one of the coordinate axes coincides with a principal axis of the permittivity tensor and the displacement vector is constant along that axis, the resultant two-dimensional equations are

$$\begin{bmatrix} D_1 \\ D_2 \end{bmatrix} = \begin{bmatrix} \varepsilon_{11} & \varepsilon_{12} \\ \varepsilon_{12} & \varepsilon_{22} \end{bmatrix} \begin{bmatrix} E_1 \\ E_2 \end{bmatrix} . \tag{2}$$

In the absence of free charge, $\bar{\nabla} \cdot \bar{D} = 0$. Therefore

$$\frac{\partial}{\partial x_1} (\varepsilon_{11}E_1 + \varepsilon_{12}E_2) + \frac{\partial}{\partial x_2} (\varepsilon_{12}E_1 + \varepsilon_{22}E_2) = 0. \tag{3}$$

But

$$E = - \nabla\phi . \tag{4}$$

Hence

$$\varepsilon_{11} \frac{\partial^2\phi}{\partial x_1^2} + 2\varepsilon_{12} \frac{\partial^2\phi}{\partial x_1 \partial x_2} + \varepsilon_{22} \frac{\partial^2\phi}{\partial x_2^2} \tag{5}$$

The cross term in Equation (5) can be eliminated by the transformation

$$\begin{bmatrix} x_1 \\ x_2 \end{bmatrix} = \begin{bmatrix} \cos\theta & \sin\theta \\ -\sin\theta & \cos\theta \end{bmatrix} \begin{bmatrix} x_1' \\ x_2' \end{bmatrix} \tag{6}$$

a special case of the general transformation

$$[x] = [T]\,[x']. \tag{7}$$

If Equation (6) is valid, components of $\bar{D}$ and $\bar{E}$ transform in the same way and this fact is used to determine the transformation law for the permittivity tensor coefficient matrix $\bar{\epsilon}$. It is required that

$$[D] = [T]\,[D'],$$

$$[E] = [T]\,[E']. \tag{8}$$

If the primed coordinate axes coincide with the principal axes of $\bar{\epsilon}$,

$$[D'] = [\epsilon']\,[E'] \tag{9}$$

and $\bar{\epsilon}'$ is diagonal.

From Equations (8) and (2)

$$[D'] = [T]^{-1}\,[\epsilon]\,[E]. \tag{10}$$

Therefore

$$[D'] = [T]^{-1}\,[\epsilon]\,[T]\,[E']. \tag{11}$$

Comparison of Equations (11) and (9) indicates that

$$[\epsilon'] = [T]^{-1}\,[\epsilon]\,[T]. \tag{12}$$

While $\bar{D}$ and $\bar{E}$ obey the same transformation law in an orthogonal transformation, this is not always true in a transformation which does not preserve orthagonality. For example, in a transformation involving no rotation, but only a contraction

of one coordinate axis in a two-dimensional anisotropic medium, $\bar{E}$ obeys the same transformation law as the coordinates. The components of $\bar{D}$, however, are functions of <u>both</u> components of $\bar{E}$ in the untransformed system and therefore the transform for $\bar{D}$ will not be the same as for $\bar{E}$. For such a two-dimensional case, it is shown in Appendix B that the permittivity transform can not be of the same form as Equation (12). This result indicates that a spatial transform (instead of a change of coordinates in the same space) is required to transform the anisotropic problem into an isotropic problem.

Application of transformation (6) reduces Equation (5) to

$$\epsilon'_{11} \frac{\partial^2 \phi}{\partial x'^2_1} + \epsilon'_{22} \frac{\partial^2 \phi}{\partial x'^2_2} = 0. \tag{13}$$

The spatial transform (derived in Appendix A) required to reduce (13) to an ordinary differential equation is

$$\begin{bmatrix} x'_1 \\ x'_2 \end{bmatrix} = \begin{bmatrix} \left(\frac{\epsilon'_{11}}{\epsilon'_{22}}\right)^{\frac{1}{4}} & 0 \\ 0 & \left(\frac{\epsilon'_{11}}{\epsilon'_{22}}\right)^{\frac{1}{4}} \end{bmatrix} \begin{bmatrix} x''_1 \\ x''_2 \end{bmatrix} \tag{14}$$

This transformation which may be interpreted as a strain (Nye, 1957) reduces Equation (13) to Laplace's equation

$$(\epsilon'_{11}\epsilon'_{22})^{\frac{1}{2}} \frac{\partial^2 \phi}{\partial x''^2_1} + (\epsilon'_{11}\epsilon'_{22})^{\frac{1}{2}} \frac{\partial^2 \phi}{\partial x''^2_1} = 0. \tag{15}$$

While there are an infinite number of transformations which reduce Equation (13) to Laplace's equation, (14) has the unique property that it preserves the differential element of area.

Boundary Modifications

Transformations (6) and (14) have modified the boundary conditions applicable to the solution of Equation (5) in a bounded medium. The modified boundary conditions will be obtained for the case of a rectangular anisotropic medium bounded by an isotropic medium as shown in Figure 1. In the unprimed coordinate system, the coordinates of points A, B, and C are

$$\begin{aligned} &A: \left(\frac{+W}{2}, \frac{+L}{2}\right) \\ &B: \left(\frac{+W}{2}, \frac{-L}{2}\right) \\ &C: \left(\frac{-W}{2}, \frac{+L}{2}\right) \end{aligned} \tag{16}$$

In the primed coordinate system the coordinates are

$$\begin{aligned} &A: \left(\frac{W\cos\theta - L\sin\theta}{2}, \frac{W\sin\theta + L\cos\theta}{2}\right) \\ &B: \left(\frac{W\cos\theta + L\sin\theta}{2}, \frac{W\sin\theta - L\cos\theta}{2}\right) \\ &C: \left(\frac{-W\cos\theta - L\sin\theta}{2}, \frac{-W\sin\theta + L\cos\theta}{2}\right) \end{aligned} \tag{17}$$

Using Equation (14) the coordinates in the double-primed system are found to be

$$A: \left[\left(\frac{\epsilon''_{22}}{\epsilon'_{11}}\right)^{\frac{1}{4}} \frac{W\cos\theta - L\sin\theta}{2}, \left(\frac{\epsilon'_{11}}{\epsilon''_{22}}\right)^{\frac{1}{4}} \frac{W\sin\theta + L\cos\theta}{2}\right]$$

$$B: \left[\left(\frac{\epsilon''_{22}}{\epsilon'_{11}}\right)^{\frac{1}{4}} \frac{W\cos\theta + L\sin\theta}{2}, \left(\frac{\epsilon'_{11}}{\epsilon''_{22}}\right)^{\frac{1}{4}} \frac{W\sin\theta - L\cos\theta}{2}\right]$$

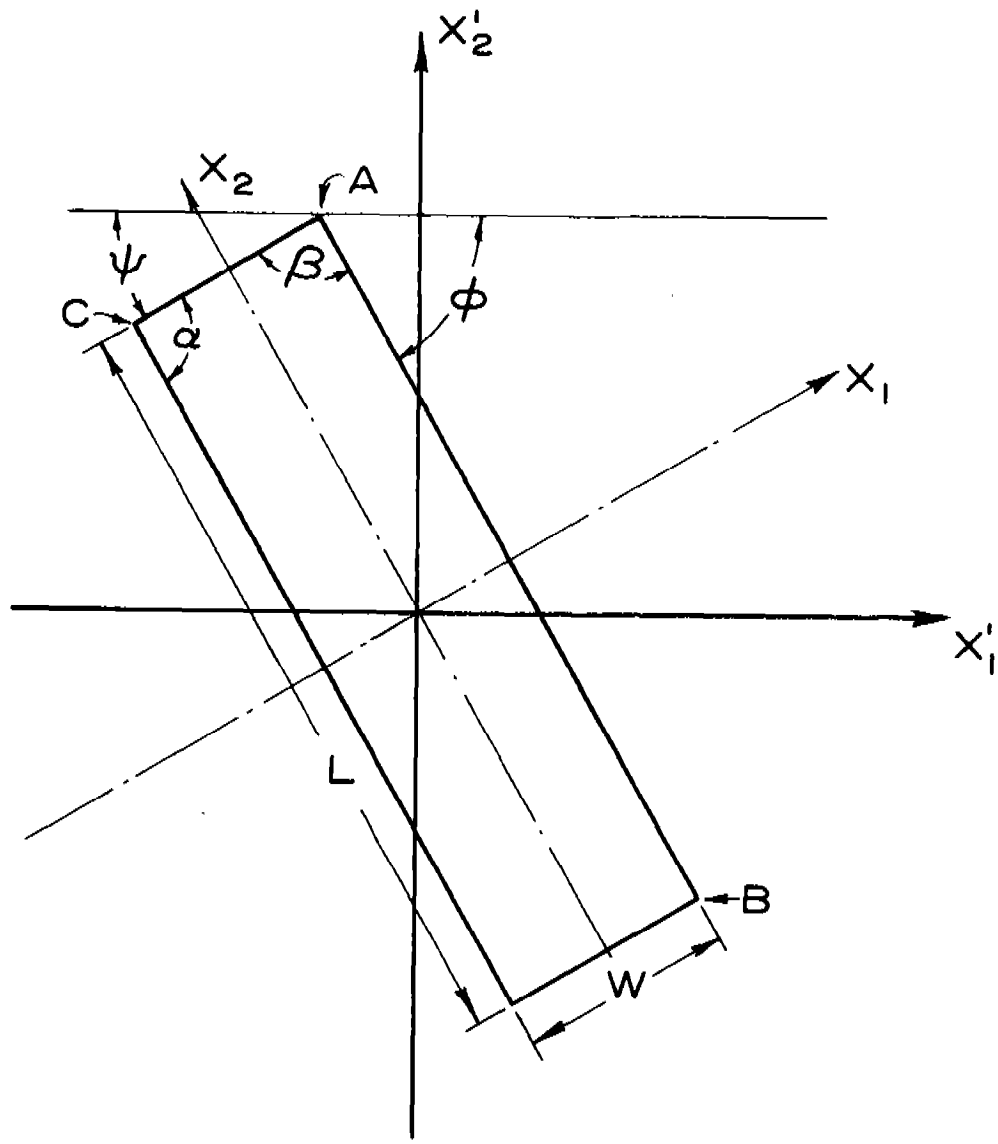

Figure I - Coordinate – Axis Designation

$$C: \left[\left(\frac{\varepsilon'_{22}}{\varepsilon'_{11}}\right)^{\frac{1}{4}} \frac{-W\cos\theta - L\sin\theta}{2}, \left(\frac{\varepsilon'_{11}}{\varepsilon'_{22}}\right)^{\frac{1}{4}} \frac{-W\sin\theta + L\cos\theta}{2}\right]. \quad (18)$$

From Figure 1 and Equation (18)

$$\alpha = \psi + \phi$$

$$\psi = \tan^{-1}\left[\left(\frac{\varepsilon'_{22}}{\varepsilon'_{11}}\right)^{\frac{1}{2}} \tan\theta\right]$$

$$\phi = \tan^{-1}\left[\left(\frac{\varepsilon'_{22}}{\varepsilon'_{11}}\right)^{\frac{1}{2}} \cot\theta\right]. \quad (19)$$

In the transformed space the dimensions L" and W" are

$$L'' = L\,\frac{(\varepsilon'_{11}\sin^2\theta + \varepsilon'_{22}\cos^2\theta)^{\frac{1}{2}}}{(\varepsilon'_{11}\,\varepsilon'_{22})^{\frac{1}{4}}}$$

$$W'' = W\,\frac{(\varepsilon'_{11}\cos^2\theta + \varepsilon'_{22}\sin^2\theta)^{\frac{1}{2}}}{(\varepsilon'_{11}\,\varepsilon'_{22})^{\frac{1}{4}}}. \quad (20)$$

Applications Of The Transformations

Gadsden constructed an anisotropy transformer from a rectangular ammonium dihydrogen phosphate (ADP) crystal cut in such a way that one axis of the crystal coincided with one of the principal axes of the permittivity tensor. The plane faces parallel to this axis were oriented at an angle of 45° with respect to the other principal axis of the permittivity tensor. As shown in Figure 2, the coincident axes are taken to be in the X_3 direction. Under the assumption of constant potential in the X_3

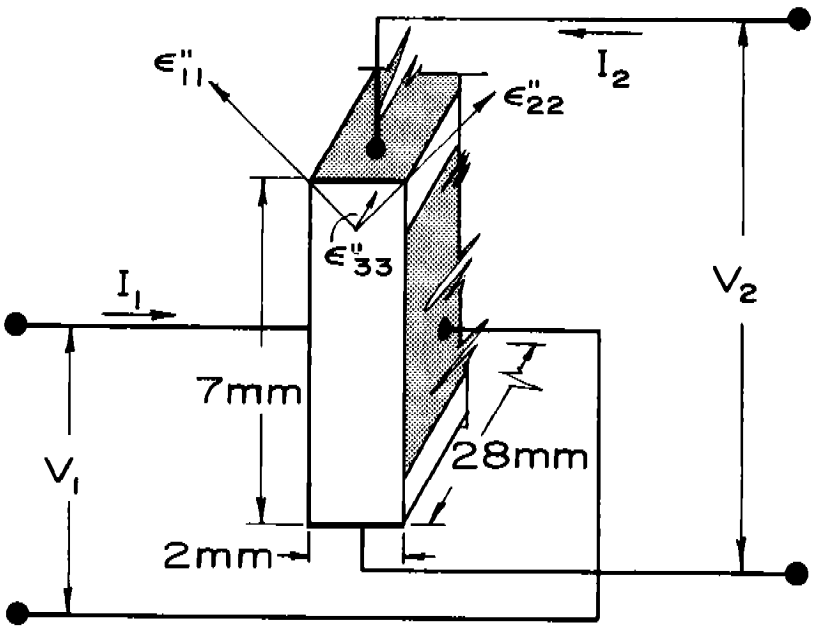

Figure 2- The Anisotropy Transformer

direction Equation (5) may be used to analyze this device. Since θ is 45°, Equations (19) and (20) reduce to

$$\alpha = 2 \tan^{-1} \left[\left(\frac{\epsilon'_{22}}{\epsilon'_{11}} \right)^{\frac{1}{2}} \right],$$

$$\frac{L''}{W''} = \frac{L}{W} \quad . \tag{21}$$

Gadsden described the anisotropy transformer with the parameters C_1, C_2, and C_m according to the circuit shown in Figure 3. The equations for this model are

$$i_1 = C_1 \dot{v}_1 + C_m \dot{v}_2$$

$$i_1 = C_m \dot{v}_1 + C_2 \dot{v}_2 . \tag{22}$$

The circuit model for the resistance-paper (teledeltos) analog of this device is shown in Figure 4 and the corresponding circuit equations are

$$I_1 = G_1 V_1 + G_m V_2 ,$$

$$I_2 = G_m V_1 + G_2 V_2 . \tag{23}$$

The similarity of Equations (22) and (23) establishes an analogy between terminal measurements of capacitance on the ADP crystal and terminal measurements of conductance on the teledeltos analog. The expression for conductance as determined by measurements for two parallel terminals of length L and separation W on teledeltos is

$$G = \frac{L}{\gamma W} \tag{24}$$

where γ is the specific resistivity of the teledeltos. In the

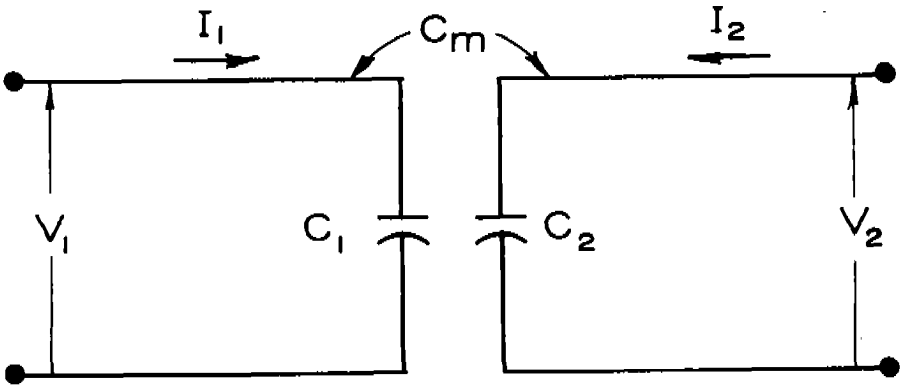

Figure 3 - Anisotropy Circuit I

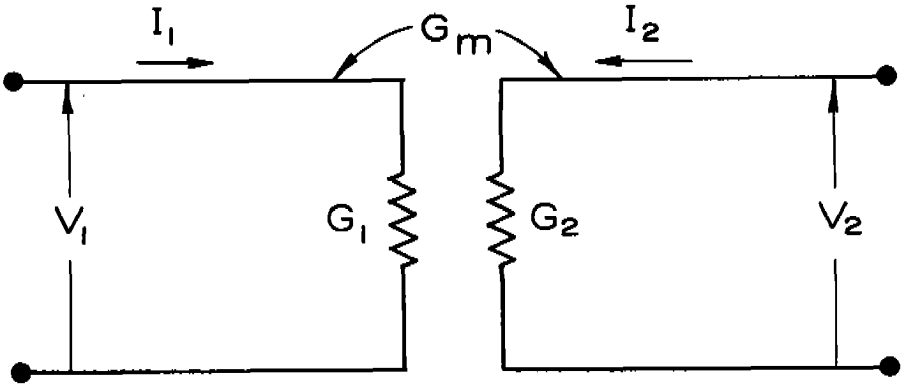

Figure 4 - The Analog Circuit

same coordinate system the expression for parallel plate capacitance per unit X_3-directed length is

$$\frac{C}{\text{unit length}} = \frac{\varepsilon'' L}{W} \quad . \tag{25}$$

Equation (15) indicates that the permittivity to be used in the double-primed system is $(\varepsilon'_{11}\varepsilon'_{22})^{1/2}$. Equations (24) and (25) establish the relation

$$C = (\varepsilon'_{11}\varepsilon'_{22})^{\frac{1}{2}} G\, d \tag{26}$$

where d is the X_3 axis length. The conductances of Equation (23) are determined by the terminal measurements

$$G_1 = \frac{I_1}{V_1}\bigg|_{V_2 = 0} \quad , \quad G_2 = \frac{I_2}{V_2}\bigg|_{V_1 = 0}$$

$$G_m = \frac{I_2}{V_1}\bigg|_{V_2 = 0} = \frac{I_1}{V_2}\bigg|_{V_1 = 0}. \tag{27}$$

The values of C_1, C_2 and C_m computed from conductance measurements on teledeltos paper (γ = 2000 / unit square) are given in Table 1 (Pilkington and Roe, 1965) along with Gadsden's experimental values for the ADP crystal shown in Figure 2.

Table 1. Comparison of Computed and Experimental Values

	C_1	C_2	C_m	Gain
Teledeltos	25.2 pF	6.1 pF	3.7 pF	0.53
Experimental	22.6 pF	7.9 pF	4.5 pF	0.5

The teledeltos and experimental values are in reasonable agreement considering that commericially available teledeltos is inhomogeneous and 15% to 20% anisotropic.

Optimum Configurations

Unfortunately the lumped parameter model of Figure 3 is not well suited for a determination of the configuration giving maximum gain or mutual capacitance because it does not completely specify the device (it does not give the results of all possible terminal measurements of capacitance) and is not easity related to the structural characteristics of the device. A lumped-parameter model which will represent any terminal measurements of capacitance is shown in Figure 5. It is based on the physical appearance of the teledeltos analog. The equality of certain interface capacitances as shown in Figure 5 is dictated by the symmetry of the crystal cut. This equivalent circuit is not unique. For example C_{13} could be replaced by a capacitor C_{24}. The decision as to which capacitance is to be used is determined by terminal measurements on the actual device. If C_{13} is chosen and the capacitance from 2 to 4 is actually the larger (or vice versa) then C_{13} will be computed to be negative. While this in no way affects the terminal characteristics of the model it clearly discourages interpretations of the circuit-model parameters in terms of the structural characteristics of the device.

The forward open-circuited voltage gain is, from Figure 5,

$$F = \frac{V_{24}}{V_{13}} = \frac{C_A - C_B}{C_A + C_B} \tag{28}$$

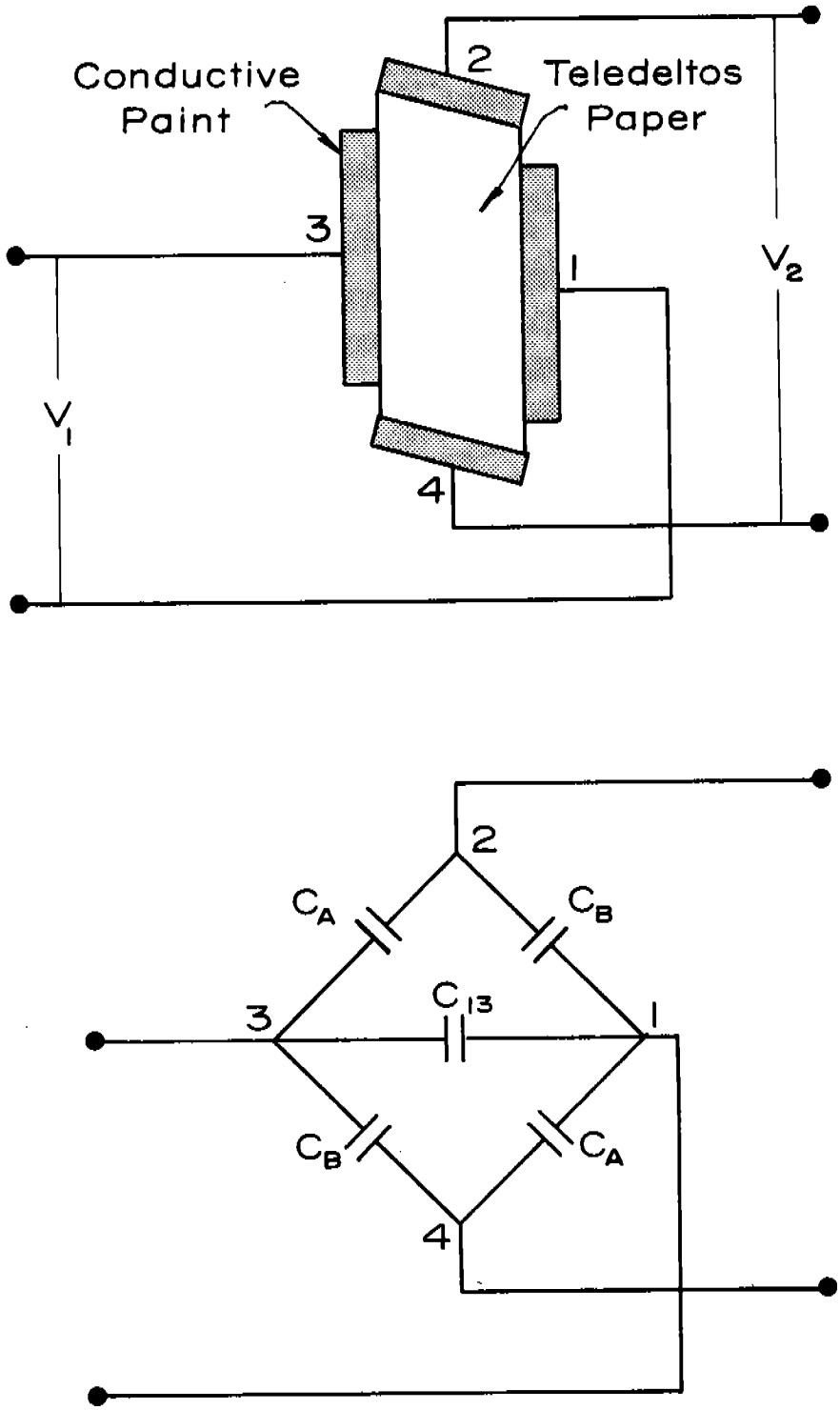

Figure 5 - Teledeltos Analog and Anisotropy Circuit.

The reverse open-circuit voltage gain is

$$R = \frac{V_{13}}{V_{24}} = \frac{C_A - C_B}{C_A + C_B + 2C_{13}} \quad . \tag{29}$$

By standard methods (Weinberg, 1962), the parameters of Figure 5 may be related to Gadsden's equivalent-circuit parameters. These relations are

$$C_1 = \frac{1}{2}(C_A + C_B + 2C_{13})$$

$$C_2 = \frac{1}{2}(C_A + C_B)$$

$$C_m = \frac{1}{2}(C_A - C_B) \quad . \tag{30}$$

Consideration of Figure 5 and Equations (30) indicates the significance of a negative C_m. If terminal measurements give an apparently negative C_m, an irrational choice of reference terminals at the output has been made (i.e., a choice giving a voltage rise from the reference at one terminal pair and a voltage drop at the other).

Maximizing C_m maximizes the gain. This is equivalent to maximizing C_A and minimizing C_B. From Figure 4, it is seen that this may be accomplished by minimizing the angle α. For ϵ'_{11} not equal to ϵ'_{22} it can be deduced from Equations (19) that a θ angle of 45° gives the minimum α. Thus a 45°-cut crystal with a large $\epsilon'_{11} - \epsilon'_{22}$ ratio should be chosen if the greatest mutual capacitance and voltage gain are to be achieved. The upper limit of the forward voltage gain is unity and is approached only in the limit as $\epsilon'_{11}/\epsilon'_{22}$ approaches infinity.

Since the linear-mode gain was found to be limited to unity, an investigation of the nonlinear properties of an anisotropic dielectric (Rochelle salt) was undertaken.

Chapter III

NONLINEAR PROPERTIES OF ANISOTROPIC DIELECTRICS

Many anisotropic materials used in the construction of devices such as those described in Chapter II are found to exhibit nonlinear dielectric properties. Materials which exhibit an electrically-reversible spontaneous polarization and dielectric hysteresis are termed ferroelectric. Figure 6 is a plot of polarization as a function of applied voltages on the ferroelectric axis of Rochelle salt ($NaKC_4H_4O_6 \cdot 4H_2O$).

Some of the compounds ferroelectric along a single crystalline axis are Rochelle (or Seignette) salt and the compounds XH_2R where X may be the potassium or ammonium groups and R the phosphate or arsenate group. These materials are piezoelectric as are all ferroelectrics. The members of the phosphate-arsenate group of ferroelectrics have Curie points below 200°K. The most widely used ferroelectric, barium titanate, is ferroelectric along all three crystalline axes (though not at the same temperature) and is not available in large single crystals. Rochelle salt has an upper Curie temperature of 255°K and is available in large single crystals (Cady, 1964). Thus Rochelle salt is, insofar as device fabrication and equipment requirements are concerned, the ferroelectric crystal most easily studied.

The interest in the polarization -E nonlinearity of these

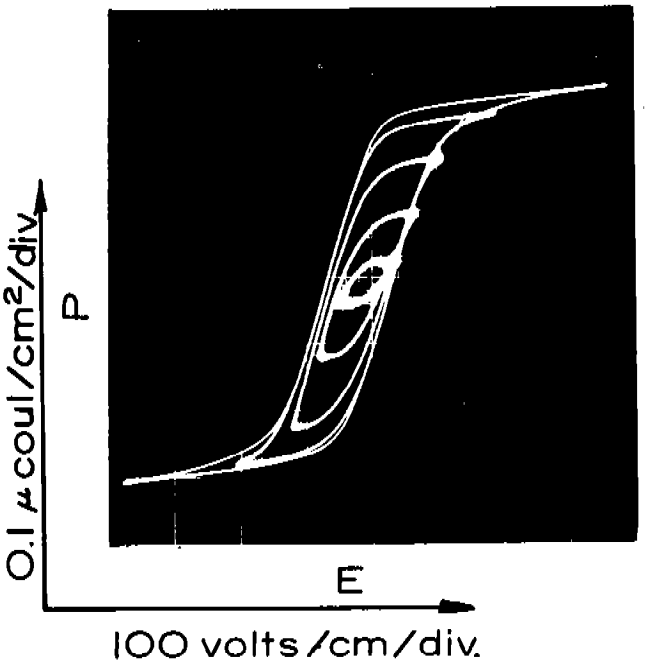

Temperature: 0°

Frequency: 60 H_z

Figure 6 - Rochelle-Salt Hysteresis Curves, X-Cut.

materials lies in the fact that control of their dielectric constants is possible. This possibility encourages the investigation of the control of anisotropic coupling by the application of an external signal.

Theories of Ferroelectricity

It is unfortunate that there is no theory of the ferroelectric properties of Rochelle salt which allows the prediction of dynamic terminal parameters. The similarity of the behavior of Rochelle salt and the other ferroelectrics to ferromagnetic materials let to an attempt to explain their behavior on the basis of a theory modeled after the classical Langevin-Weiss theory of ferromagnetism. An elementary molecular model in which H_2O molecules formed rotating dipoles was developed (Jaynes, 1953). However, the effect of piezoelectric interaction was not considered in this theory. In addition, the structure of Rochelle salt was, at that time, undetermined. Thus it was not possible to specify the dipole interactions on which the theory was based. More recent internal field theories of Rochelle salt have involved the motion of hydrogen bonds within the molecules (Jona and Shirane, 1962) but as the structure determination is as yet incomplete these theoretical models do not allow the calculation of terminal parameters for arbitrary configurations. The phenomenological thermodynamic treatment of Mueller (Cady, 1964) allows the calculation of terminal parameters for z-cut crystals with faces normal to the ferroelectric axis. While in principle the effect of fields not parallel to the ferroelectric axis could be calculated, a number of difficulties are present.

Mueller's theory is developed for fields parallel to the ferroelectric axis. If the crystal is cut at an angle (other than 90°) with respect to this axis the partial differential equation (5) of Chapter II must be solved with appropriate boundary conditions to obtain the ferroelectric-axis field. Moreover the equation is nonlinear since the ferroelectric-axis dielectric constant is field dependent. Känzig (1957) has noted that "the anisotropy of some ferroelectrics is so high that the direction of the spontaneous polarization cannot deviate much from the ferroelectric axis." For Rochelle salt the mechanism for polarization reversal is considered by Känzig to be a decrease and reversal along the ferroelectric axis only. However, Mason (1950a) indicates that the off-axis dielectric constants for Rochelle salt may be found by the rotation transformation which was discussed in Chapter II. Any attempt to determine theoretically the effects of fields not parallel to the ferroelectric axis would appear to require a reformulation of Mueller's theory as well as an increased understanding of the mechanism of polarization reversal in ferroelectrics. The investigation of nonlinear properties is therefore restricted to experimental studies of nonlinear coupling in Rochelle salt.

Crystal Preparation and Properties

In addition to the desireable properties of Rochelle salt (room temperature ferroelectric range, availability of large single crystals, high anisotropy) there are several properties which engender difficulty for an investigator. Rochelle salt is hygroscopic, deliquescent, temperature sensitive, pressure sensi-

tive, brittle, and subject to aging of the electrical and mechanical properties. Samples must be prepared and handled with utmost care and maintained in a near-ideal environment.

All crystals used in this work were manufactured by Clevite Corporation. Dimensions before cutting were 5 mm x 5 mm x 50 mm with the 50 mm dimension along the z axis. Both 0°-cut (ferroelectric axis normal to two faces of the crystal) and 45°-cut crystals were used. Crystals were sectioned perpendicular to the z axis giving a finished length of about 22 mm. Before electrodes were attached the crystal surfaces were polished with water, then cleaned with distilled water or ethanol. Surfaces not to be covered with electrodes were masked with high dielectric strength tape and fine-grain silver conductive epoxy adhesive was spread on the areas to be electroded. After setting of the adhesive, the tape masks were removed. Electrode thicknesses were approximately 0.2 mm. Damping due to electrode mass was not sufficient to cause any observable distortion of polarization hysteresis curves.

The crystals were mounted in a spring-clip holder which fit in a temperature test chamber. The spring clip pressure was not sufficient to cause any observable distortion of polarization hysteresis loops. The test chamber had a temperature range of 250°K to 315°K controllable by varying current input to the thermoelectric cooler units. The test chamber temperature was measured with a Chromel-Alumel thermocouple.

In spite of all efforts some crystal contacts were initially defective or became defective during the course of the investigation. This was usually caused by corrosion between the surface of the crystal and the contacts or the formation of condensate on the crystal surface and the consequent loosening of the contacts.

Measurements on crystals with a thin layer of low-dielectric-constant material between the contacts and the crystal surface are virtually worthless because of the high dielectric constant of Rochelle salt. For example, surface contamination of only 0.001 mm on a 10 mm crystal of Rochelle salt can cause the measured value of the ferroelectric-axis dielectric constant to be in error by as much as 10 per cent (Cady, 1964a). In this work, crystal contacts were considered acceptable if the polarization hysteresis loop taken parallel to the ferroelectric axis at 60 Hz indicated that saturation polarization was reached with fields of 200 volts/cm or less. According to Mason's internal field theory for Rochelle salt (1950b), the coercive field necessary to reverse the polarization of a single domain is on the order of 100 volts/cm. The field strength at closure of the hysteresis loop is typically twice the coercive field. Saturation polarization as used here, is the magnitude of the polarization at the point of closure of the loop.

Surface conduction due to the formation of Rochelle salt solution at the surface of the crystal under humid conditions can alter considerably the appearance of hysteresis curves. In such cases leakage widens the loop and increases the value of the field intensity at which saturation polarization appears to occur. The Mueller modification (1935) of the circuit introduced by Sawyer and Tower (1930) compensates for leakage by incorporating a phase control. A description of this circuit is given in Appendix C. However, for most measurements the leakage was held at levels sufficiently low that this correction was not needed.

Outside the ferroelectric range of Rochelle salt (255°K to 297°K) hysteresis disappears but a nonlinear P - E (polarization

electric field intensity) relation exists for several degrees outside the upper and lower Curie points.

For small fields (less than 200 volts/cm) the static dielectric constant exhibits a sharp maximum at the upper and lower Curie points and is almost constant over the range of 263°K to 283°K. The thermal conductivity of Rochelle salt is several times lower than that of quartz (Cady, 1964a) and crystals are slow in attaining thermal equilibrium. Repeatable measurements are possible only if several hours have elapsed since a temperature change. Because internal heating occurs during the course of an experiment, the crystal temperature rises above that of the chamber. Therefore, the chamber temperature was held in the range of -5°C to 0°C. In this region the dielectric constant does not vary rapidly with temperature and the d-c resistance is typically 10^9 ohms or greater.

Application of Ferroelectric Properties

An examination of dielectric hysteresis loops indicates that a number of device concepts associated with square-loop magnetic materials are applicable to ferroelectrics. Figure 7 is a circuit diagram for one of the simplest dielectric amplifiers which can be constructed (Katz, 1959). In this amplifier the control signal biases the ferroelectric sample to various points of the hysteresis loop and thereby controls the impedance which appears at the terminals of the a-c power source. In addition to the difficulties associated with the material properties of ferroelectrics (large hysteresis losses, high coercive forces, temperature sensitivity and aging) there is the problem

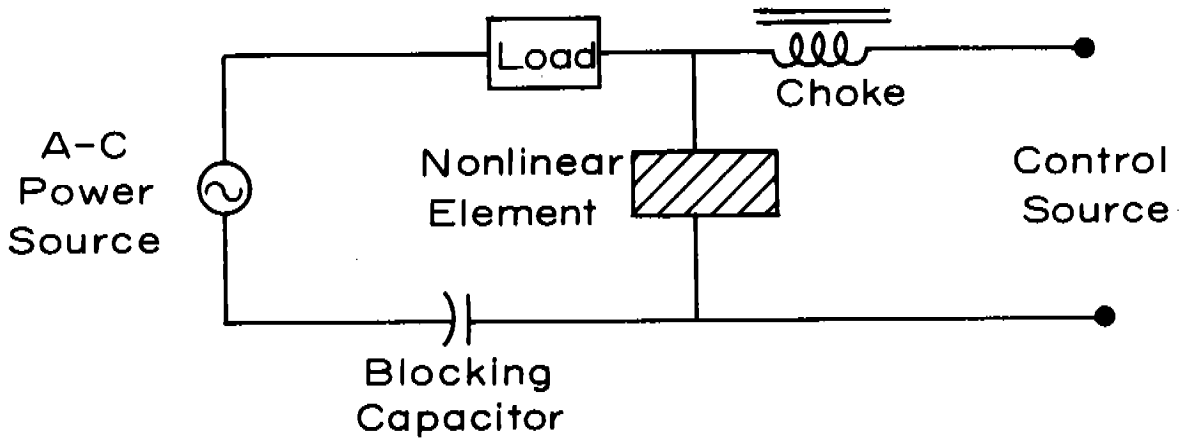

Figure 7 - Basic Dielectric Amplifier

of isolating the control source from the power source. In the circuit of Figure 7 a blocking capacitor is necessary to prevent shorting of the control source by the power source. The choke prevents shorting of the nonlinear element by the control source.

The four-terminal crystal configurations of Chapter II have the property that ideal voltage sources at the input and output are partially isolated by the crystal impedance. A major objective of this experimental investigation is the development of four-terminal crystal configurations with dielectric constants controllable by the application of an external signal and providing inherent isolation of the power sources.

Effects Of Electrical Biases

The application of a d-c voltage to a 0°-cut crystal under test in a Sawyer-Tower circuit was found by David (1935) to produce a shift in the origin of the hysteresis loop. David was able to demonstrate the equivalence of mechanical and electrical bias. A set of electrically biased hysteresis loops and the circuit with which they were measured are shown in Figures 8 and 9. The parallel d-c bias is the most direct method of control of the dielectric constant and is the basis of operation of the dielectric amplifier of Figure 7.

Biases On 0°-Cut Crystals

In this investigation the first four-terminal crystal configuration considered was 0°-cut with electrodes on the faces perpendicular and parallel to the ferroelectric axis.

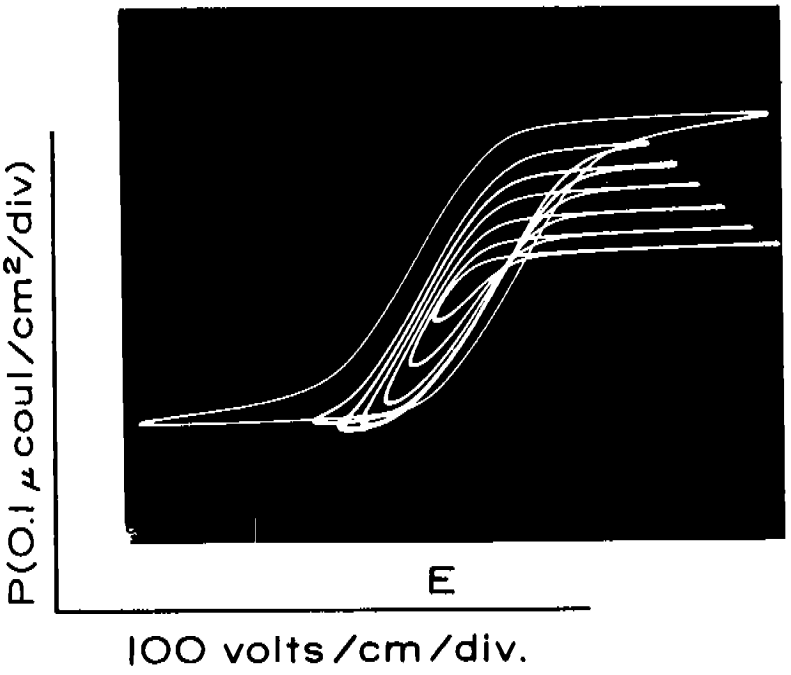

Bias Voltages: 0, 22.5, 45.0, 77.5, 90.0, 112, and 135 volts

Temperature: 7° C

Frequency: 60 H_z

Figure 8- Biased Hysteresis Curves, X-Cut Rochelle Salt.

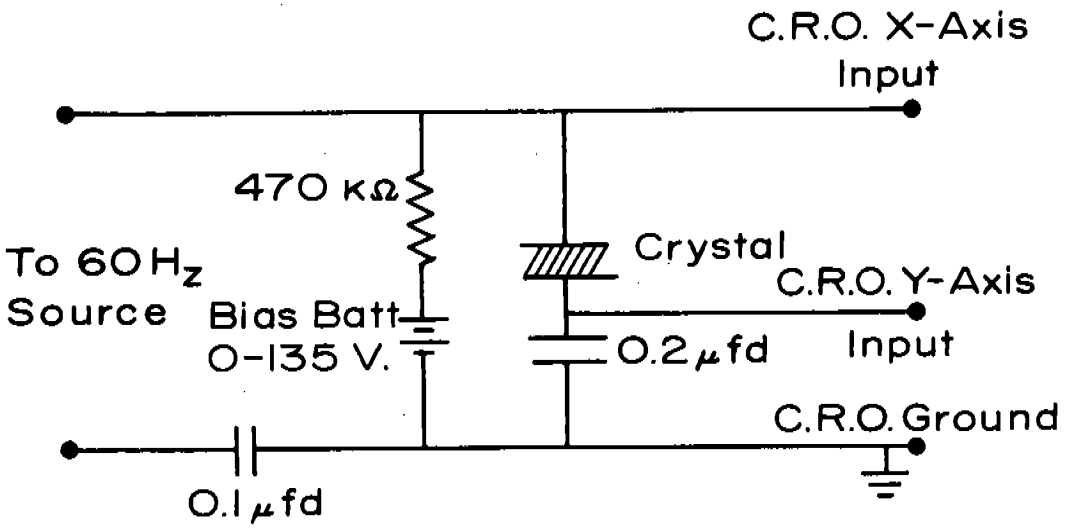

Figure 9 - Measurement Circuit for Curves of Fig.8.

For a 0°-cut crystal no anisotropic coupling between fields parallel and perpendicular to the ferroelectric axis is expected. However, a ferroelectric interaction due to partial alignment of ferroelectric domains by fields perpendicular to the ferroelectric axis might be expected to distort hysteresis curves taken parallel to the ferroelectric axis. Experimentally this effect is not observed.

Biases On 45°-Cut Crystals

The full electrode and partial electrode 45°-cut crystals of Figure 10 were the next configurations to be investigated. Polarization hysteresis loops (these are given as q-v loops since the specification of electrode area and spacing is ambiguous for any but 0°-cut crystals) taken between various faces of a 45°-cut crystal are shown in Figure 11. It was found that hysteresis loops between A and D were in no way affected by loads or biases at terminals B and C. However, the application of a resistive load to terminals B anc D was found to cause the appearance of a hysteresis curve between terminals A and C in contrast to the absence of any marked nonlinearity in the unloaded measurement. The hysteresis loops taken between terminals A and C were dependent on both the resistive load and any bias voltage on terminals B and D. A set of hysteresis loops for various loads and biases is presented in Figure 12 for the partial-electrode 45° configuration. The effect of bias is similar for the full electrode configuration.

For the partial-electrode crystal the open-circuit voltage gain (both forward and reverse) at 60 Hz was within three per cent of the maximum of 1.0. No distortion was observable at the output

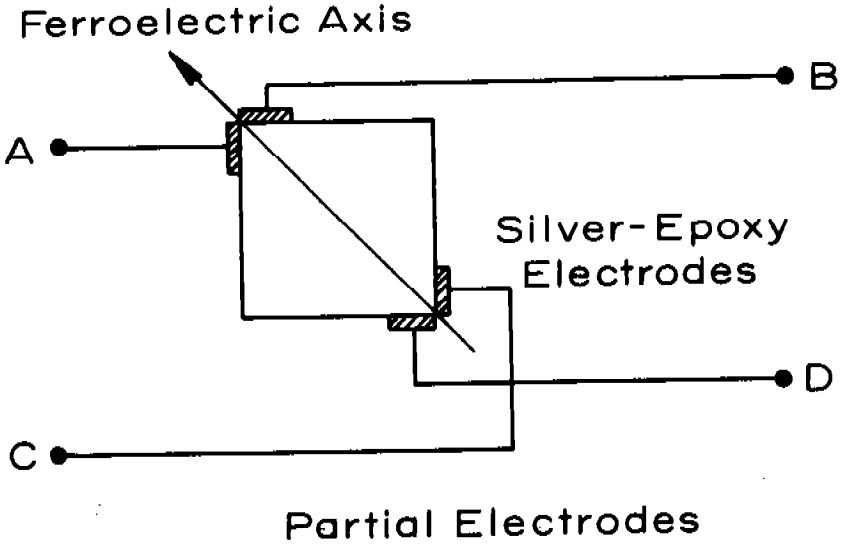

Partial Electrodes

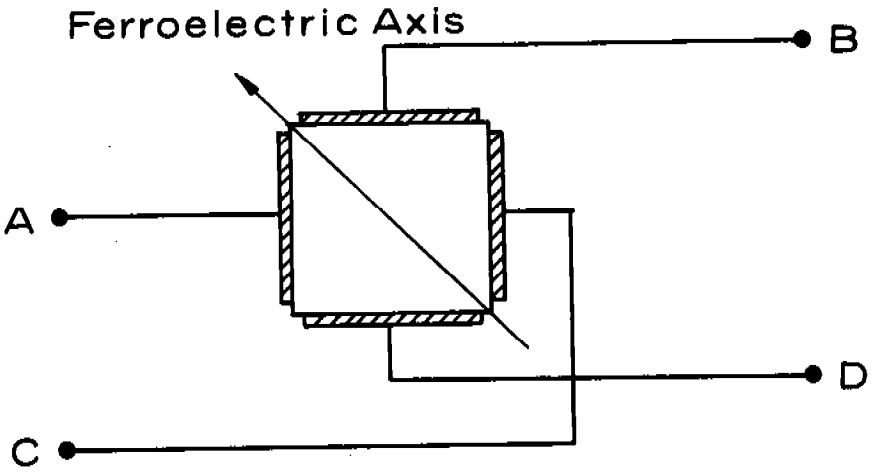

Full Electrodes

Figure 10 - 45°- Cut Crystal Configurations

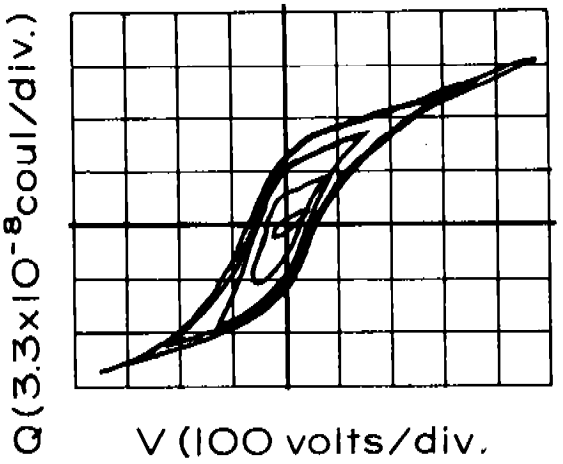

Terminals A and D

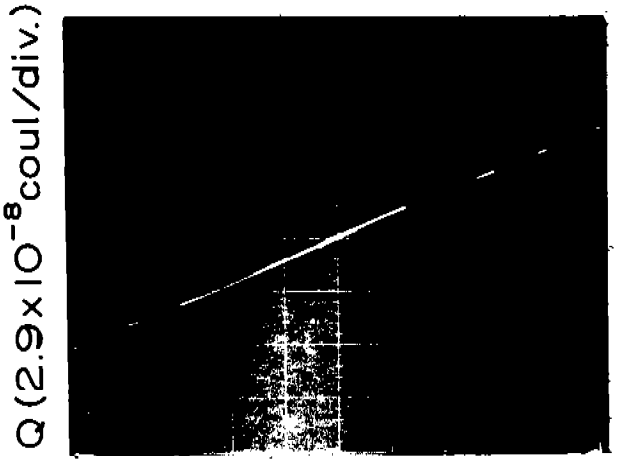

Terminals A and C
B-D Open

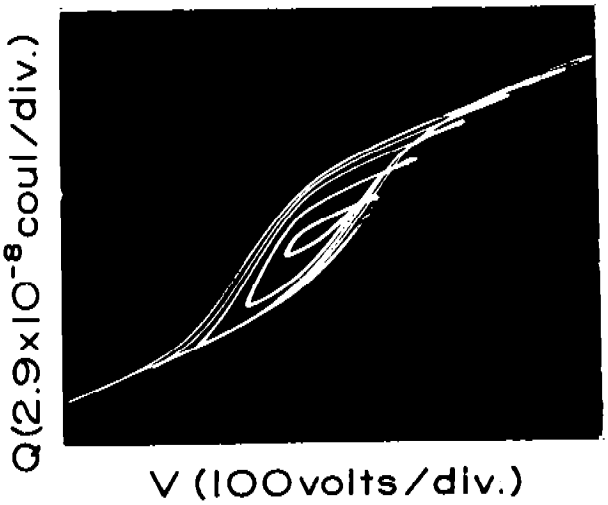

Terminal A and C
B-D Shorted

Figure 11 - Hysteresis Curves, 45°-Cut Crystal

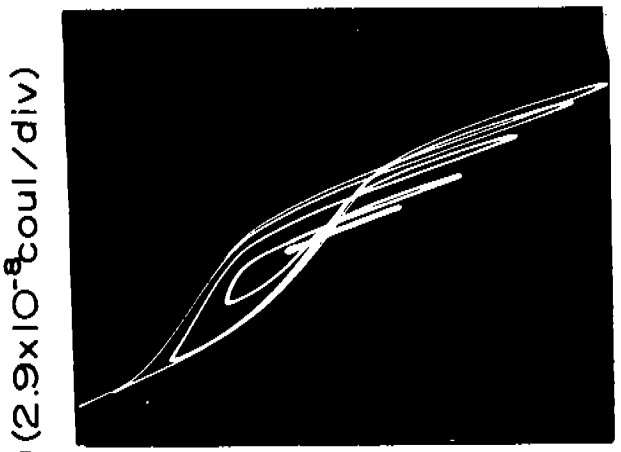

Taken Between Terminals A and C. 1 Meg Ω Load On B-D, 90 Volts Bias.

Taken Between Terminals A and C 9.4 Meg Ω Load on B-D, 90 Volts Bias.

Temperature: 5° C.
Frequency: 60 H_z

Figure 12 - Loaded and Biased 45°-Cut Crystal, Partial Electrodes.

terminals.

The full-electrode crystal had lower gain than the partial-electrode crystal and considerable distortion was present in the output waveform. Figure 13 shows the voltages appearing between various terminals of the crystal for a sinusoidal source voltage.

The fraction of a d-c bias voltage which appears at the input terminals of a four-terminal crystal is dependent on the load across the input terminals. For a dielectric amplifier as shown in Figure 7, this is the series resistance plus the internal impedance of the power source. Figure 14 demonstrates the change in d-c transfer ratio as the shunt impedance at the input terminals changes. The resistances (shunted by 35 pF) are those appearing at the input of an electrometer.

Figure 14 indicates that the bias transfer ratio is insignificant for resistances customarily encountered in power sources. Although such a low transfer ratio is desireable insofar as isolation is concerned, the origin of this effect increases the problems associated with the material properties of the crystal. Reference to the polarization hysteresis curves indicates that the presence of a resistive load at the bias terminals increases the losses in the crystal. The removal of this loss component is not possible since it is by the presence of a resistive load at the bias terminals that input-output coupling is achieved.

Device Applications At Low Frequencies

The biased hysteresis loops for the 45° configuration demonstrated the possibility of construction of a dielectric amplifier functioning on the same principle as the one shown in

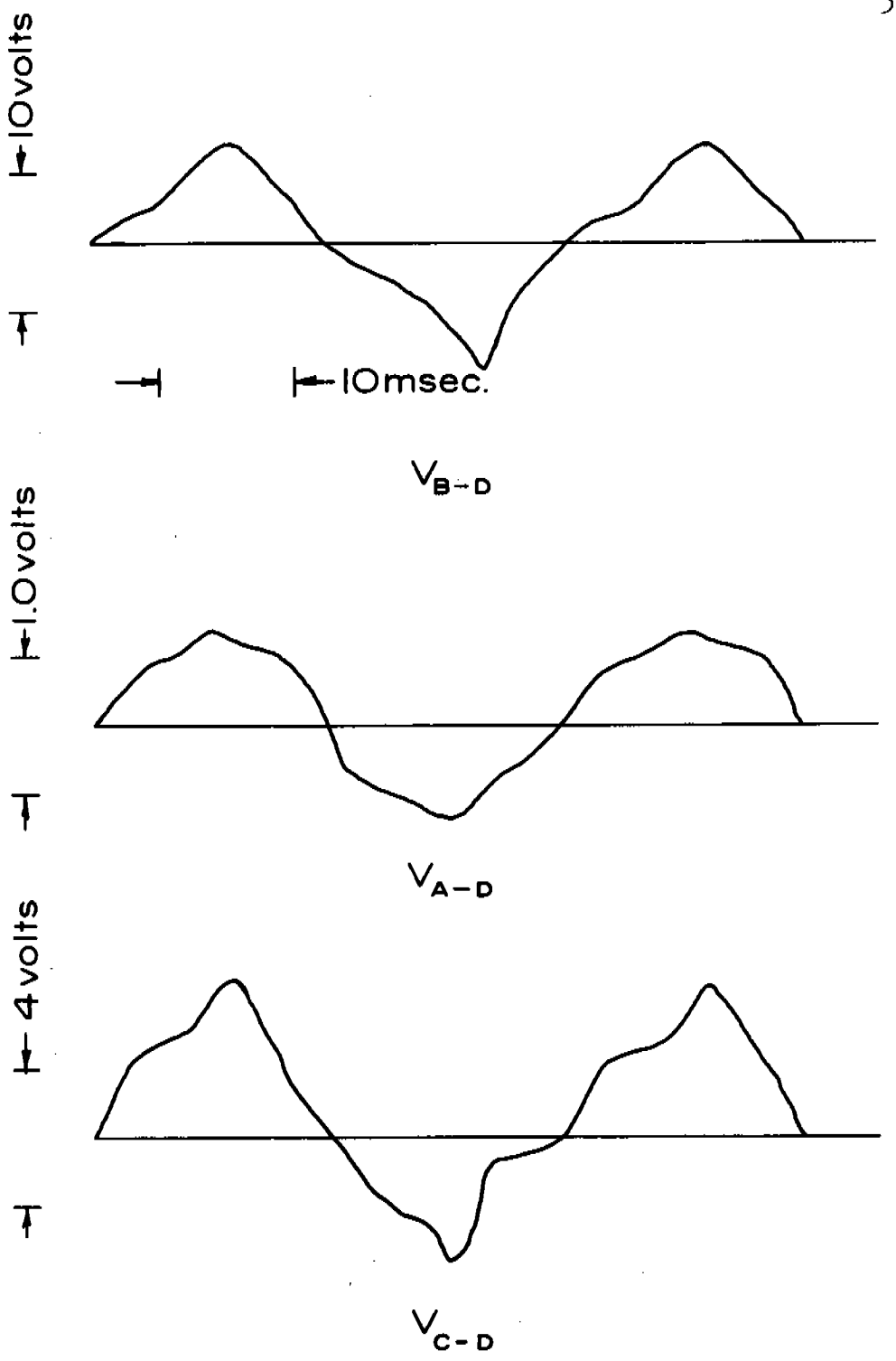

Figure 13 – Transfer Characteristics, Full Electrode 45°-Cut Crystal

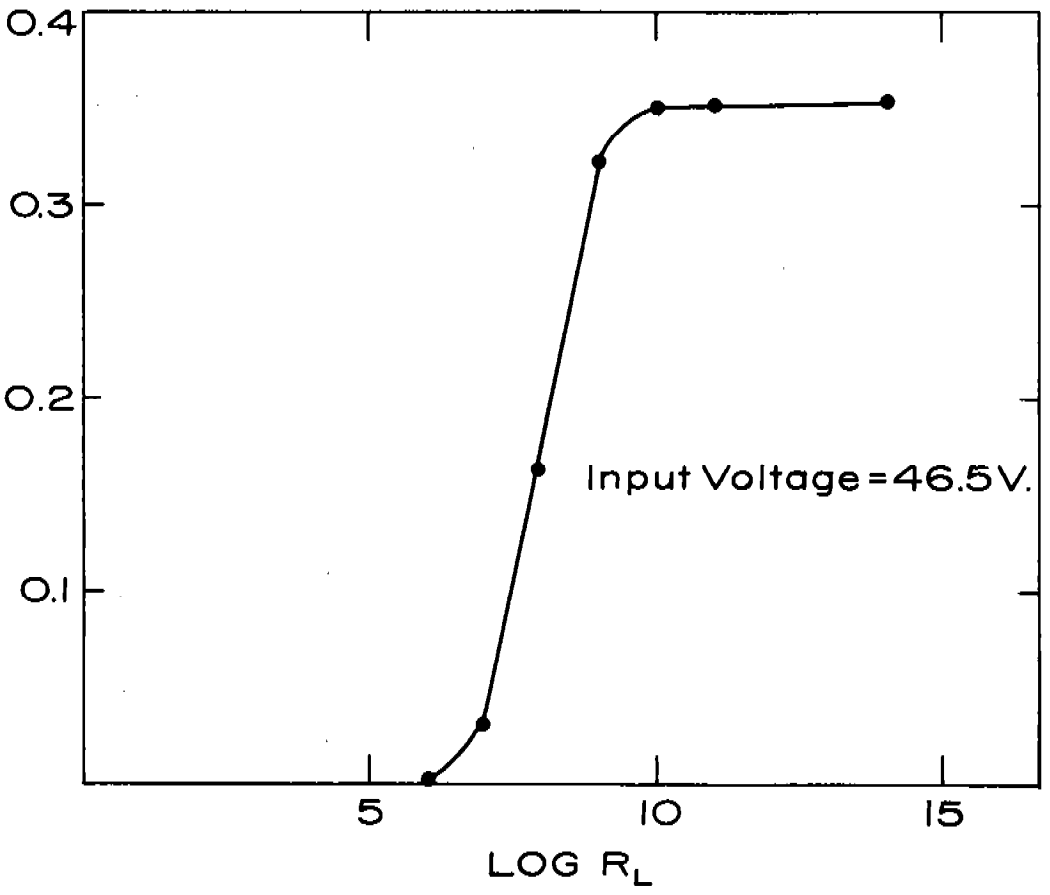

Figure 14 – D-C Transfer Characteristic

Figure 7. The circuit shown in Figure 15 was employed to test this conclusion.

In the circuit of Figure 15, a particular choice of input voltage, load resistance and frequency is determined by the following considerations: the source voltage impressed on the crystal must be sufficient to drive it into saturation; the impedance of the crystal must be of the same order of magnitude as that of the series resistor since the crystal is to be a control element; the power-source frequency must be less than the lowest resonant frequency of the crystal so that the ferroelectric nonlinearity is not obsucred by piezoelectric effects. The bias resistor R_B was included to eliminate any effects attributable to a change in impedance of the bias source as bias batteries were changed. Curves of voltage across the load resistance as a function of d-c bias voltage are given in Figure 16. For measurement purposes it was necessary to use an isolated 500 Hz source.

Because there is a preferred direction of polarization for these crystals the effects of positive (defined as being in the direction of preferred polarization) and negative bias are not identical. The application of a positive bias causes an increase in the impedance of the crystal as it would in the case of a symmetrical hysteresis curve, but the application of a negative bias causes an initial decrease in the crystal impedance and then an increase as the crystal bias is increased. The steady-state current flow from the bias source is so small that it may be attributed to the conduction current flow through the crystal. For temperatures near 0°C the d-c resistance of the particular crystals used was on the order of 10^9 ohms. Except for this conduction current loss, the only input to the bias terminals is that

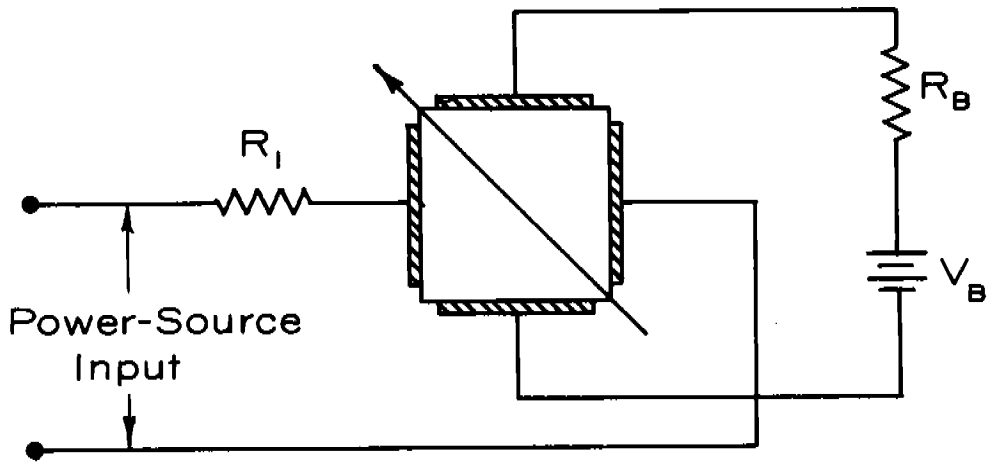

Figure 15 - Dielectric Amplifier Test Circuit

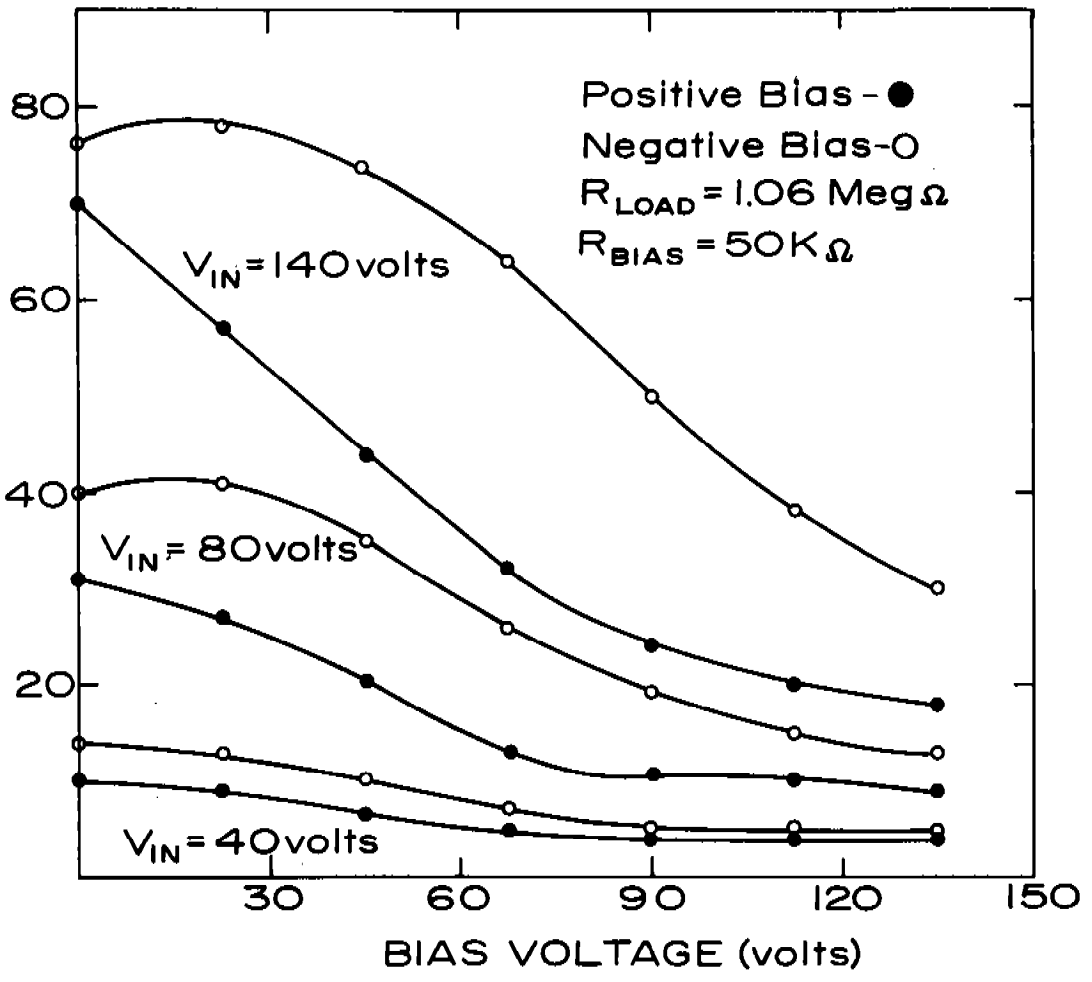

Figure 16 - Dielectric Amplifier Transfer Characteristic.

required to charge the capacitance appearing at the bias terminals to the voltage of the bias battery.

High-Frequency Applications

The extension of the operating range of ferroelectric devices to high frequencies is limited by the increase in dielectric loss with frequency increase and by the piezoelectric effect always present in ferroelectric crystals. The frequency dependence of polarization hysteresis is illustrated in Figure 17. These hysteresis curves indicate the increased coercive forces and dielectric losses which have limited the power-source and control-source frequencies of dielectric amplifiers. The curves of Figure 17 were taken parallel to the ferroelectric axis of a 45°-cut crystal. Polarization-hysteresis curves for 0°-cut crystals have been given by Hablutzel (1939). Polarization hysteresis data for 45°-cut crystals was limited to frequencies below 50KHz because the crystals melted before saturation polarization could be reached at higher frequencies.

The piezoelectric effect for fields less than about 10 volts/cm or along crystalline axes exhibiting no polarization hysteresis may be described by capacitance measurements. In Figure 18 the capacitance between terminals A and C of a crystal cut as indicated in Figure 10 is given. The intense resonance at 200 KHz and higher harmonics is found experimentally to prohibit control of the dielectric constant in the resonance regions. When voltage greater than 30 volts rms were applied with frequencies slightly above or below the mechanically resonant frequency, an audio beat was coupled to the atmosphere demonstrating

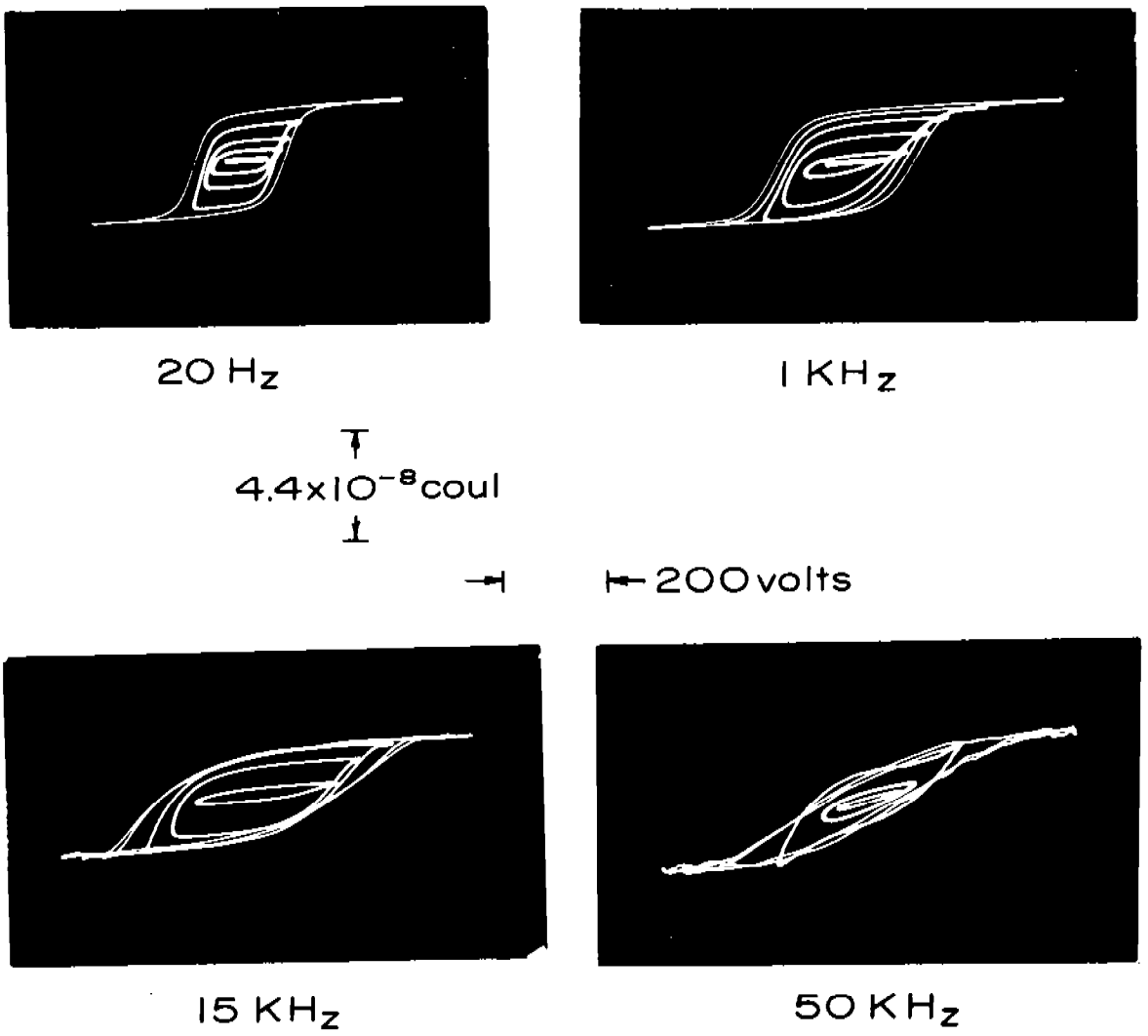

Figure 17- Frequency Dependence of Polarization Hysteresis.

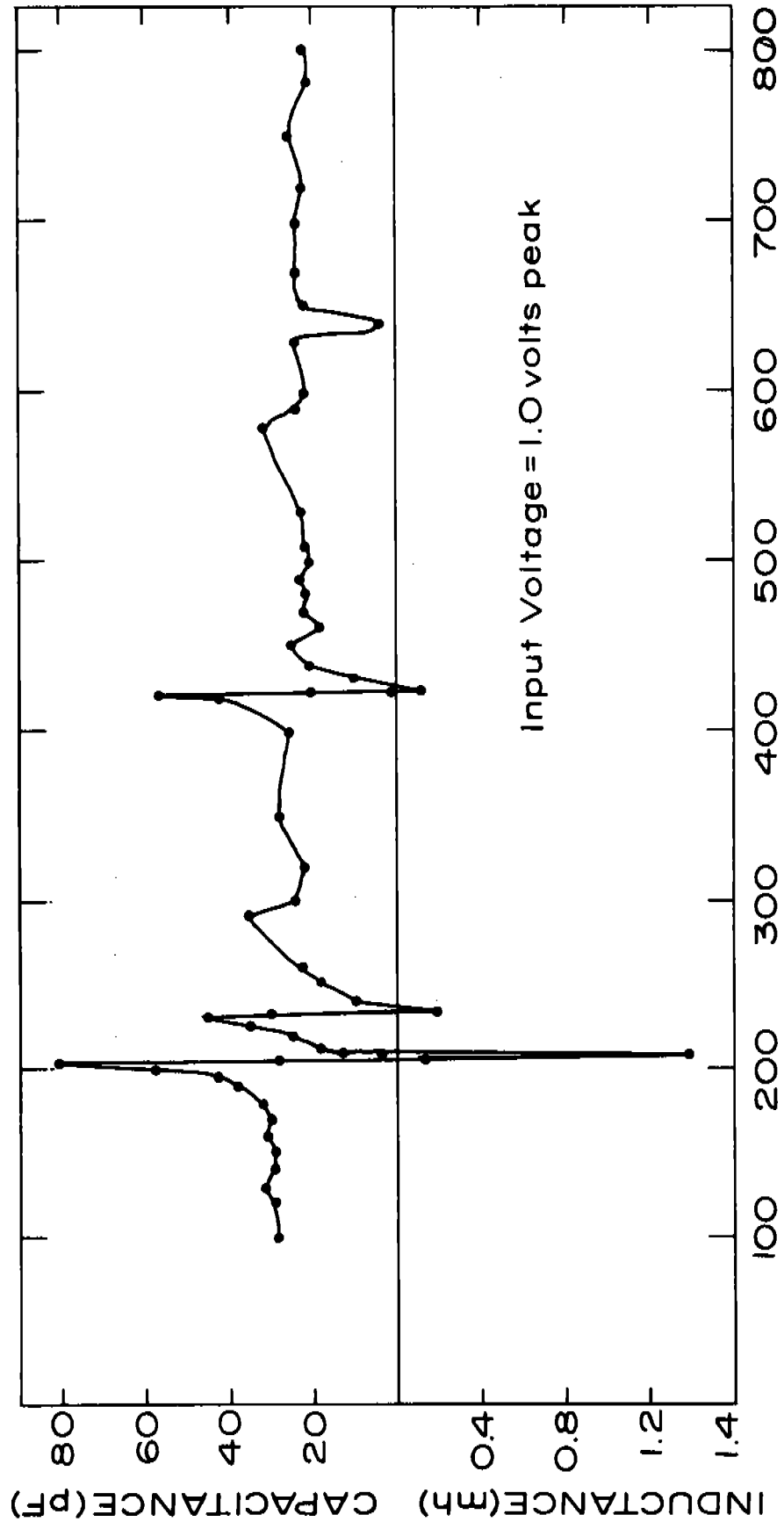

Figure 18- Frequency Dependence of the Terminal Capacitance

the electrical and mechanical interaction in the crystal. With reference to Figure 18, a source frequency of 700 KHz was chosen as being relatively free of piezoelectric effects. The crystal properties were investigated using an inductor in series with the crystal and series resonant with the crystal capacitance at 700 KHz. This technique proves useful because the Q of the resonant circuit effectively increases the gain of the configuration.

In dielectric amplifier configurations a choice must be made as to the relative amplitudes of the control signal and the power-source signal. One of these must be large enough to saturate the nonlinear element. If, for example, the power-source saturates the nonlinear element on each half cycle, the control signal then determines what fraction of the polarization-hysteresis loop is traversed. Alternatively, a power-source voltage much smaller than that needed to saturate the nonlinear element may be used. In this case the control signal determines where on the major P-E loop a minor P-E loop will be executed by the power-source signal. For small-signal source operation the dielectric losses are determined by the frequency and amplitude of the larger control voltage. If the power source saturates the nonlinear element and low-level control voltages are used, the dielectric losses are determined by the frequency and amplitude of the power-source voltage. The power-source frequency is always chosen to be greater than the highest control-source frequency. Therefore the condition of low-level power-source signal gives the lowest dielectric loss, but the high-level control signal then supplies dielectric losses in the crystal.

The mode of operation of the series resonant configuration shown in Figure 19 may be explained in terms of the biased

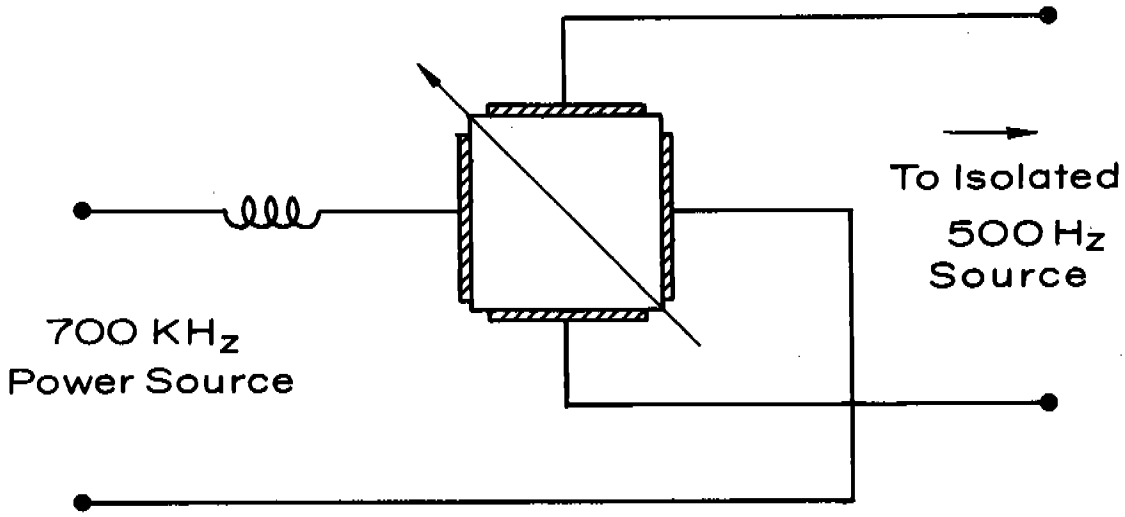

Figure 19 - Series Resonant Configuration

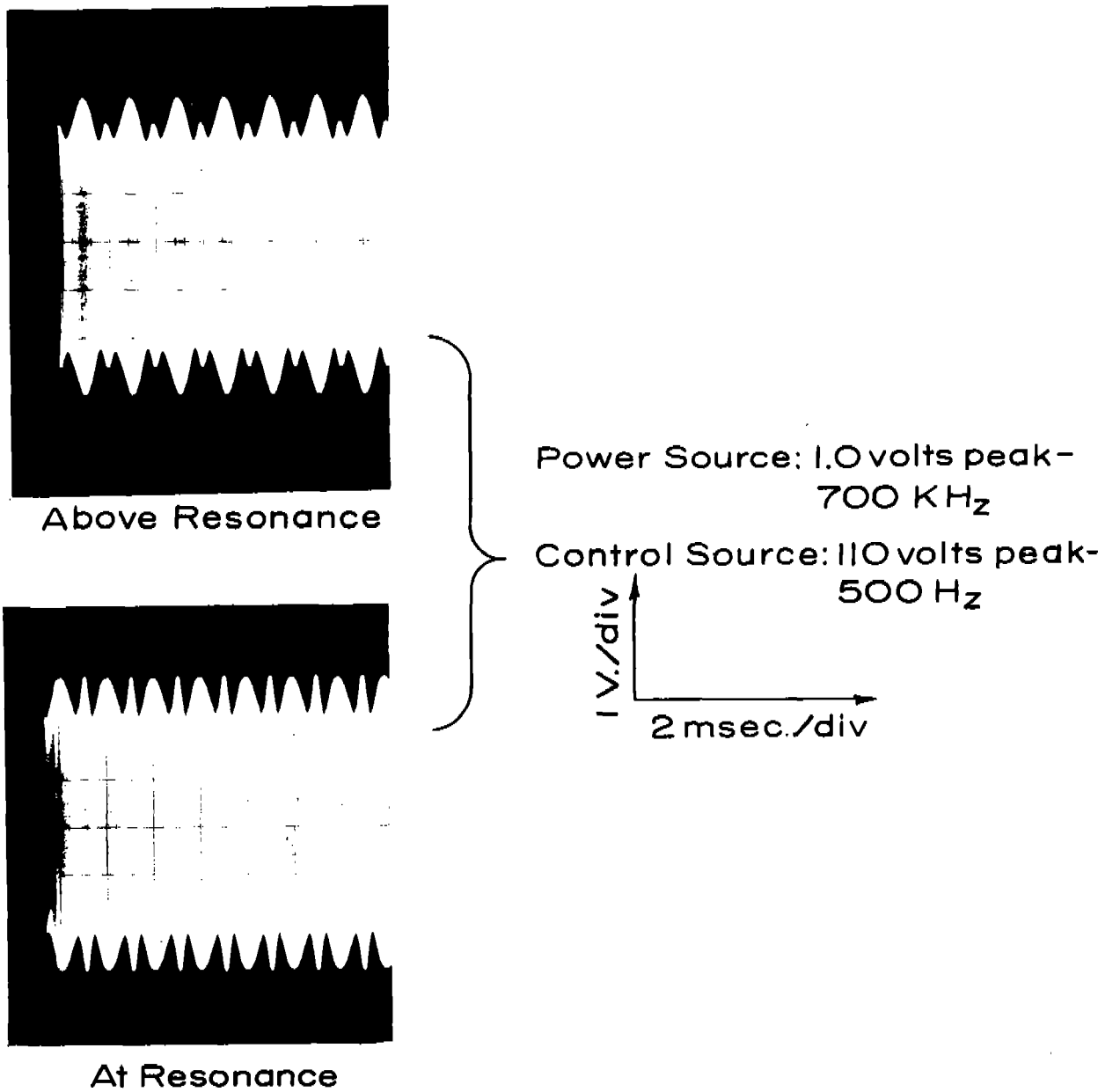

Figure 20 - Modulation of the Power-Source Signal.

Chapter IV

DISCUSSION AND CONCLUSIONS

Linear Anisotropic Dielectrics

In Chapter II a technique for the analysis of fields in linear anisotropic dielectrics was developed. Applications of the technique are not so restricted as its origin would indicate. It is useful for the analysis of boundary-value problems described by equations reducible to Laplace's equation. In addition to anisotropic dielectrics, materials having anisotropic thermal or electrical conductivities might be analyzed.

The use of analog field mapping is not an integral part of the transformation process. The transformation to an isotropic space changes the boundaries of an anisotropic medium but not the terminal properties. Thus the terminal capacitances of an anisotropy transformer are equal to those of the proper warped isotropic dielectric.

As a consequence of the existence of this transformation, it is concluded that no linear anisotropic dielectric configuration can achieve a voltage gain greater than unity by the mechanism of anisotropic coupling.

Origin Of The Rochelle Salt Terminal Properties

The explanations of the functional mechanisms of the various nonlinear crystal configurations studied in Chapter III are incomplete. They are consistent with the experimental results but give no indication of the internal mechanism producing the observed terminal properties. Among the effects to be explained are: the appearance and disappearance of polarization nonlinearity as the 45° configuration was loaded and unloaded; the absence of polarization nonlinearity along axes only a few degrees off the ferroelectric axis (partial-electrode 45°-cut crystal); the relative magnitudes of the 0°-cut and 45°-cut saturation polarization voltages; and the marked nonlinearity of the transfer voltages of the full electrode 45° configuration. All of these effects may be explained by extending Kanzig's statement that "the polarization cannot deviate much from the ferroelectric axis." It will be assumed that no deviation of the polarization from the ferroelectric axis is possible. This implies that the dielectric constant is not representable by a second-rank tensor but has a singularity in the direction of the ferroelectric axis.

The experimental results of Chapter III and the preceding assumptions suggest, for oriented configurations, the model shown in Figure 21. The linear capacitances are much smaller than the nonlinear capacitances since the "average" ferroelectric-axis dielectric constant is typically three or more orders of magnitude larger than the other dielectric constants. In the absence of a connection between terminals B and D, only a small polarization nonlinearity between terminals A and C would be expected. This is because most of the applied voltage is dropped across the linear

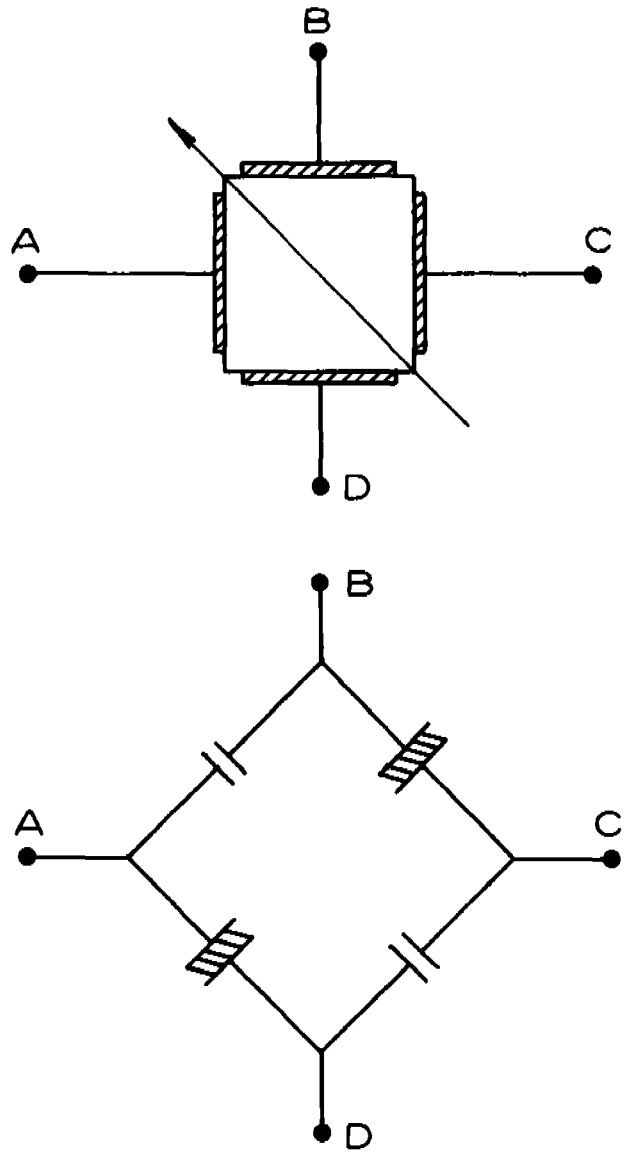

Figure 21 - The Nonlinear Equivalent Circuit.

elements. With B shorted to D, the polarization hysteresis loop between A and C should have twice the saturation-polarization voltage of--and be similar in shape to--the polarization hysteresis loop between A and D. These results are in agreement with the hysteresis loops of Figure 11. The nonlinear voltage transfer characteristics of the full-electrode 45° configuration are seen to arise from the spacing variation of the electrodes A and D. This variation results in different saturation polarization voltages for various parts of the crystal. It should be noted that the model is not applicable when the applied fields are along the ferroelectric axis. The equivalent circuit is based on the postulate of no internal field interaction for applied fields off the ferroelectric axis. The effect of the mechanism of anisotropic coupling on the terminal properties of Rochelle salt is negligible.

The equivalent circuit indicates that an oriented crystal of Rochelle salt may be represented, for purposes of dielectric amplification, as a number of 0°-cut crystals. Thus oriented configurations of Rochelle salt may be used interchangeably with multiple-terminal 0°-cut crystals for applications in dielectric amplification.

Utility Of Multi-Terminal Elements

From the experimental and theoretical results one must conclude that devices using nonlinear anisotropic coupling in Rochelle salt are not practicable. It should be emphasized that this conclusion is valid only for Rochelle salt and the practicability of any oriented configuration is dependent on the mechanism

of polarization reversal in the dielectric material. Unfortunately, little consideration has been given to the macroscopic consequences of the mechanism of polarization reversal in ferroelectric crystals. The concept of anisotropic coupling in multiterminal elements is, like all dielectric amplifier techniques, a method in search of a material.

APPENDIXES

Appendix A

SPATIAL TRANSFORM DERIVATION

It is desired to transform the elliptic differential equation

$$\epsilon'_{11} \frac{\partial^2 \phi}{\partial x'^2_1} + \epsilon'_{22} \frac{\partial^2 \phi}{\partial x'^2_2} = 0 \tag{A1}$$

into an equation of the form

$$\epsilon_z \frac{\partial^2 \phi}{\partial z_1^2} + \epsilon_z \frac{\partial^2 \phi}{\partial z_2^2} = 0 \tag{A2}$$

Let

$$\begin{bmatrix} x'_1 \\ x'_2 \end{bmatrix} = \begin{bmatrix} k_1 & 0 \\ 0 & K_2 \end{bmatrix} \begin{bmatrix} z_1 \\ z_2 \end{bmatrix} \tag{A3}$$

Then

$$\frac{\partial^2 \phi}{\partial x'^2_1} = \frac{1}{k_1^2} \frac{\partial^2 \phi}{\partial z_1^2}$$

$$\frac{\partial^2 \phi}{\partial x_2^2} = \frac{1}{k_2^2} \frac{\partial^2 \phi}{\partial z_2^2} \tag{A4}$$

Combining (A1) and (A4) gives

$$\frac{\epsilon'_{11}}{k_1^2}\frac{\partial^2\phi}{\partial z_1^2} + \frac{\epsilon'_{22}}{k_2^2}\frac{\partial^2\phi}{\partial z_2^2} = 0 \qquad \text{(A5)}$$

The additional condition required for the evaluation of the transform matrix is that

$$dx'_1\, dx'_2 = dz_1 dz_2 \qquad \text{(A6)}$$

which is equivalent to the restriction that

$$k_1 k_2 = 1 \qquad \text{(A7)}$$

Both (A6) and (A7) express the requirement that transformation (A3) be orthagonal. From (A5) and (A7)

$$\frac{\epsilon'_{11}}{k_1^2} = \frac{\epsilon'_{22}}{k_2^2} = \epsilon_z ,$$

and

$$k_1 = \left(\frac{\epsilon'_{11}}{\epsilon'_{22}}\right)^{\frac{1}{4}} .$$

Therefore

$$k_1 = (\epsilon'_{11}/\epsilon'_{22})^{\frac{1}{4}} , \quad k_2 = (\epsilon'_{22}/\epsilon'_{11})^{\frac{1}{4}} , \qquad \text{(A8)}$$

and

$$\epsilon_z = (\epsilon'_{11}\epsilon'_{22})^{\frac{1}{2}} . \qquad \text{(A9)}$$

Appendix B

THE PERMITTIVITY TRANSFORM

In Chapter II it was demonstrated that for a rotation of coordinate axes the $[\epsilon]$ transformation required is

$$[\epsilon_z] = [T]^{-1} [\epsilon'] [T] \tag{B1}$$

where [T] is the coordinate transformation. That (B1) is not the required transformation may be seen by choosing

$$[T] = \begin{bmatrix} a & 0 \\ 0 & b \end{bmatrix} . \tag{B2}$$

From (B1) and (B2)

$$[\epsilon_z] = \begin{bmatrix} \frac{1}{a} & 0 \\ 0 & \frac{1}{b} \end{bmatrix} \begin{bmatrix} \epsilon'_{11} & 0 \\ 0 & \epsilon'_{22} \end{bmatrix} \begin{bmatrix} a & 0 \\ 0 & b \end{bmatrix}$$

$$[\epsilon_z] = [\epsilon'] . \tag{B3}$$

Hence transformation (B1) cannot be a valid $[\epsilon]$ transform since the z space is required to be isotropic.

The correct transform is

$$[\epsilon_z] = [T]^{-1} [\epsilon'] [T]^{-1} . \tag{B4}$$

Appendix C

ANALYSIS OF THE SAWYER-TOWER CIRCUIT

The circuit shown in Figure 22 is Mueller's modification of a circuit introduced by Sawer and Tower and is commonly used for measurement of ferroelectric-hysteresis curves (Sawyer and Tower, 1930). In this circuit C_3 is chosen to be much larger than the maximum capacitance of the crystal so that the impedance of C_3 is always much less than that of the crystal. The voltage across C_3 which drives the vertical amplifier of an oscilloscope is given by

$$v_3 = \frac{1}{C_3} \int i \, dt = \frac{A}{C_3} \int \frac{dD}{dt} \, dt$$

$$v_3 = \frac{A(\epsilon_0 E + P)}{C_3} \approx \frac{AP}{C_3} \qquad (C1)$$

Approximation (C1) is valid along the x axis of Rochelle salt since $P >> \epsilon_0 E$. The voltage across C_2 which drives the horizontal amplifier of an oscilloscope is sinusoidal since the source voltage is sinusoidal. The resultant hysteresis loop is not a correct one because the voltage across the crystal is not sinusoidal. This error is minimized, however, by insuring that the impedance of C_3 is always much less than that of the crystal.

While not shown in the circuit diagram the d-c resistance

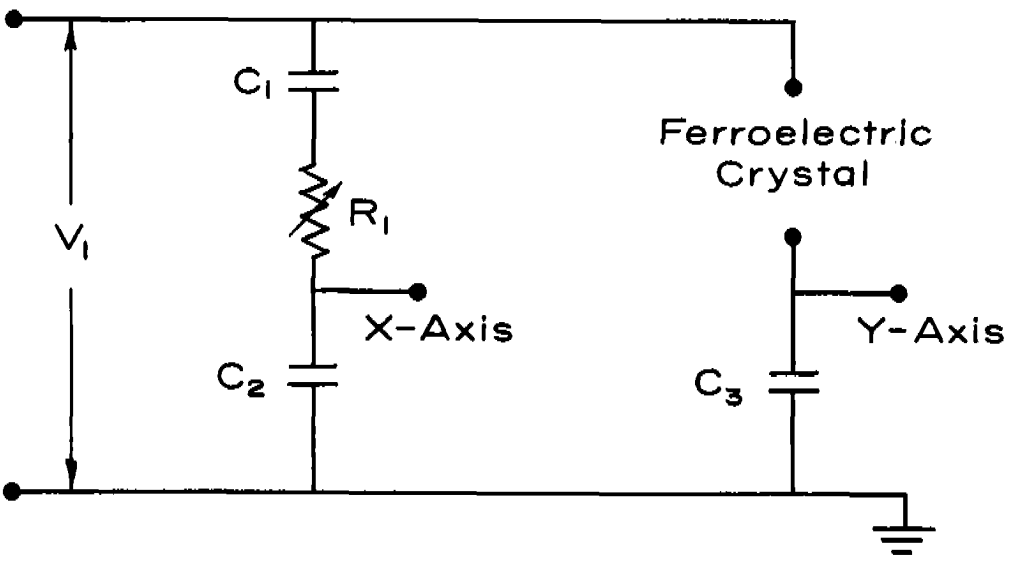

Figure 22 — The Sawyer-Tower Circuit.

of the crystal may be represented as a series resistance R_x. The effect of phase control R_1 may best be analyzed by replacing the crystal with a linear capacitance C_x in series with a linear resistance R_x. The voltage across C_2 is given by

$$V_H = \frac{V/J\omega C_2}{R_1 + 1/J\omega C_a} \qquad (C2)$$

where

$$C_a = \frac{C_1 C_2}{C_1 + C_2} . \qquad (C3)$$

The voltage across C_3 is

$$V_v = \frac{V/J\omega C_3}{R_x + 1/J\omega C_b} \qquad (C4)$$

where

$$C_b = \frac{C_x C_3}{C_x + C_3} . \qquad (C5)$$

Equations (C2) and (C4) may be rewritten in phasor notation as

$$V_v = \frac{VC_a}{C_2(1 + \omega^2 R_1^2 C_a^2)^{1/2}} \, \tan^{-1}\omega R C_a ,$$

$$V_H = \frac{VC_b}{C_3(1 + \omega^2 R_x^2 C_b^2)^{1/2}} \, \tan^{-1}\omega R_x C_b . \qquad (C6)$$

Since the linear capacitance which has been substituted for the crystal may exhibit no hysteresis,

$$R_1 C_a = R_x C_b . \qquad (C7)$$

Substitution of Equations (C3) and (C5) gives

$$R_I = \frac{R_x C_x C_3 (C_1 + C_2)}{C_1 C_2 (C_x + C_3)} \approx \frac{R_x C_x (C_1 + C_2)}{C_1 C_2} \qquad (C8)$$

The ideal dielectric hysteresis loop should enclose an area equal to the cyclic energy loss due to the nonlinear P - E relation in the material. If all losses in addition to this were representable by a constant series resistance the correct hysteresis curve could be obtained by saturating the sample and adjusting R_1 to give a straight line on the saturation portion of the hysteresis curve since C_x is constant on this portion of the curve. This is what is done in practice but the resultant hysteresis curve is not exact because there is a voltage dependent component of R_x which represents the vibrational losses in the crystal. Since the vibrational losses vary with the driving voltage they cannot be exactly compensated for by the phase resistor R_1. As long as saturated hysteresis curves are being sought, the inclusion of these losses is tolerable since R_1 is adjusted by examining the saturation portion of the hysteresis curve. For unsaturated hysteresis curves no such reference is available and phase adjustment is a matter of experience.

LIST OF REFERENCES

LIST OF REFERENCES

Cady, W. G. 1964. Piezoelectricity. Chap. 20-26. Dover Publications Inc. New York.

David, R. 1935. Dependence of the dielectric properties of Rochelle salt on mechanical conditions. Helv. Ph. Ac. 8: 431-84.

Gadsden, C. P. 1963a. The anisotropy transformer. Proc. IEEE. 51: 612-13.

Gadsden, C. P. 1963b. Correction to the anisotropy transformer. Proc. IEEE. 51: 952.

Hablutzel, J. 1939. Dielectric investigations of heavy-water Rochelle salt. Helv. Ph. Ac. 12: 489-510.

Jaynes, E. T. 1953. Ferroelectricity. Chap. 1. Princeton Univ. Press. Princeton.

Kanzig, W. 1957. Ferroelectrics and antiferroelectrics. Solid State Physics. 4:110-11.

Jona, F., and Shirane, G. 1962. Ferroelectric Crystals. Chap. 7. Macmillan Co. New York.

Katz, H. W. 1959. Solid State Magnetic and Dielectric Devices. Chap. 8. John Wiley and Sons, Inc. New York.

Loh, Y. P. 1963. A preliminary study of dielectric anisotropy transformers. Unpublished MS thesis, Tulane University.

Mason, W. P. 1950a. Piezoelectric Crystals and Their Application to Ultrasonics. p. 459. D. Van Nostrand Co., Inc. New York.

Mason, W. P. 1950b. Piezoelectric Crystals and Their Application to Ultrasonics. Chap. 11. D. Van Nostrand Co.,Inc. New York.

Mueller, H. 1935. Properties of Rochelle salt. Phys. Rev. 47: 175-91.

Nye, J. F. 1957. Physical Properties of Crystals. p. 76, 201. Oxford Univ. Press. London.

Pilkington, T. C., and Roe, R. B. 1965. Analysis of fields in anisotropic media with application to the anisotropy transformer. Proc. IEEE. 51: 643-54.

Sawyer, C. B., and Tower, C. H. 1930. Rochelle salt as a dielectric. Phys. Rev. 35:269-73.

Weinberg, L. 1962. Network Analysis and Synthesis. Chap. 1. McGraw-Hill Book Co., Inc. New York.